High spin shell model states in the isotope $^{90}_{43}Tc_{47}$

D. Rudolph, C. J. Gross,* M. K. Kabadiyski, K. P. Lieb, and M. Weiszflog
II. Physikalisches Institut, Universität Göttingen, D-3400 Göttingen, Federal Republic of Germany

H. Grawe, J. Heese, and K.-H. Maier
Hahn-Meitner-Institut GmbH, D-1000 Berlin 39, Federal Republic of Germany

J. Eberth
Institut für Kernphysik der Universität zu Köln, D-5000 Köln 41, Federal Republic of Germany
(Received 21 October 1992)

High spin states in the nucleus ^{90}Tc have been identified for the first time via the fusion evaporation reaction ^{58}Ni(^{36}Ar,3pn)^{90}Tc, at 149 MeV beam energy. The OSIRIS spectrometer with an additional high purity Ge detector at 162° and several particle detectors were used to measure $\gamma\gamma$ and particle-$\gamma\gamma$ coincidences, directional correlations of oriented states (DCO's), and line shapes due to Doppler-shift attenuation (DSA). Furthermore, an angular distribution experiment was performed with the reaction ^{58}Ni(^{35}Cl,2pn)^{90}Tc, at 120 MeV beam energy. Some 90 transitions were placed into a level scheme comprising 45 levels reaching up to a possible spin $I = 26\hbar$ at 11.2 MeV excitation energy. Definite spin assignments for more than half of the levels were made via angular distribution coefficients and DCO ratios. Shell model calculations were performed in a restricted configuration space consisting of only the $p_{1/2}$ and $g_{9/2}$ orbitals. The level scheme can be reproduced very well up to spin $I = 21\hbar$. The predicted structure of the states is discussed and compared to those of neighboring isotopes.

PACS number(s): 21.60.Cs, 23.20.En, 23.20.Gq, 23.20.Lv

I. INTRODUCTION

Neutron deficient nuclei with mass numbers $A \approx 80$–90 and $Z \leq 40$ have been the subject of intense experimental efforts and systematic studies during the last decade. The isotopes of $34 \leq Z \leq 40$ and with $N \leq 45$ reveal excitations with pronounced rotational bands caused mostly by prolate quadrupole deformation, centered around the $N = Z$ nucleus $^{76}_{38}$Sr with $|\beta_2| \approx 0.4$ [1]. They exhibit interesting features such as shape coexistence, suppression of pairing correlations, competing proton and neutron alignments, signature inversion, or triaxiality. These features can be understood in terms of either total Routhian surface calculations, particle-rotor-models, or the interacting boson approach in the O(6) limit [2–6]. Moving toward the $N = 50$ shell closure, the $N = 46$ nuclei show distinct features of transitional nuclei. Their states can be described by a simple shell model approach, although estimated and measured $B(E2)$ values indicate collective, i.e., mainly vibrational contributions at least in the low spin region [7–9]. However, isotopes with $N \geq 47$ reveal the classic signatures of a high spin scheme dominated by seniority states associated with pure aligned single-particle excitations [10].

Recent heavy ion in-beam studies have given access to light Nb, Mo, and Tc nuclei [11–20]. These isotope chains show the occurrence of the transition between rotational and single-particle excitation mode at neutron numbers N=45,46: Lifetime measurements in the $N = 46$ nucleus ^{87}Nb indicate a decrease of collectivity when moving from the 1qp (one-quasiparticle) to the 3qp states [12] but in the $N = 45$ isobar ^{87}Mo an increase of collectivity was found [15]. However, the investigation on ^{88}Mo has shown that even four valence protons and four neutron holes with respect to $^{88}_{38}Sr_{50}$ do not drive this nucleus to a permanent ground-state deformation [16].

The present work on high spin states in ^{90}Tc continues our systematic studies of the Tc isotope chain [19,20] and extends the investigation of $N = 47$ nuclei to higher proton numbers. It should be stressed that the knowledge on the odd-A isotones ^{87}Zr [21] and ^{89}Mo [17] is fairly comprehensive, whereas the information concerning the odd-odd isotones ^{86}Y [22] and ^{88}Nb [10] is rather marginal. An extensive level scheme such as that deduced for ^{90}Tc here reveals an interesting check on residual interaction parameters when adding one more neutron hole to the better known $N = 48$ isotones [23, 24].

Apart from a β-decay study by Oxorn and Mark [25] nothing was known on ^{90}Tc at the beginning of the investigation. Very recently a preliminary excitation scheme was proposed by Wen *et al.* [26]. The experimental arrangements used in the present work and the identification of γ rays originating from ^{90}Tc are presented in Sec. II. The level scheme is described in Sec. III. The shell model interpretation including comparisons to the even-even nucleus ^{90}Mo and the odd-A neighbors ^{89}Mo

*Present address: Physics Division, Oak Ridge National Laboratory, Oak Ridge, TN 37831.

and ^{91}Tc as well as energy level systematics of the N=47 isotones is the subject of Sec. IV.

II. EXPERIMENTS

A. Identification of ^{90}Tc γ rays and $\gamma\gamma$ coincidences

The setup of the ^{58}Ni + ^{36}Ar experiment has been described in previous papers [16, 18], and therefore only a brief review is given here. A 149-MeV ^{36}Ar beam provided by the VICKSI accelerator at the Hahn-Meitner-Institut at Berlin bombarded a 99.98% enriched, 19.8 mg/cm^2 thick ^{58}Ni target foil. The resulting γ radiation was measured by the OSIRIS spectrometer [27] consisting of 12 BGO Ge detectors mounted in two rings at 65° and 115° to the beam, and an additional large volume high purity Ge detector at 162°. Evaporated charged particles were detected in four 300 μm surface barrier Si ΔE detectors and the evaporated neutrons in seven segments of the NE213 HMI neutron ball [28]. All particle detectors were positioned at forward angles. Altogether 2×10^8 events were sorted into a prompt $\gamma\gamma$ matrix; the γ-ray energy range was 50–2500 keV and the time window 20 ns. The corresponding neutron gated matrix contained about 2×10^6 events. The residual nucleus ^{90}Tc is produced in the $3pn$ evaporation channel from the compound nucleus ^{94}Pd. Its overall relative cross section amounts to 7.7(3)%. PACE2 Monte Carlo simulations [29] predict 10% relative cross section corresponding to 60 mb absolute cross section. However, ^{90}Tc provides more than 50% of all neutron gated events. Energy and efficiency calibrations of the Ge detectors were performed with ^{152}Eu and ^{133}Ba standard sources.

Intensity relations between different particle-$\gamma\gamma$ coincidences were inspected to assign γ-ray cascades to the various residual nuclei. Therefore gates were set on either known or unknown strong transitions in the $\gamma\gamma$, $n\gamma\gamma$, $2n\gamma\gamma$, $p\gamma\gamma$, and $pn\gamma\gamma$ matrix. The intensities of various transitions in these gates were used to calculate intensity ratios, such as $R_n = I(\gamma\gamma)/I(n\gamma\gamma)$, $R_{2n} = I(\gamma\gamma)/I(2n\gamma\gamma)$, $R_p = I(\gamma\gamma)/I(\mathrm{p}\gamma\gamma)$, and $R_{pn} = I(n\gamma\gamma)/I(pn\gamma\gamma)$. This gating procedure was used to rule out contaminations due to doublet structures in the total projections of the above-mentioned matrices. Yields of transitions in gates on strong γ rays in ^{87,88,90}Mo, ^{87,89}Nb, and ^{91}Tc reveal calibration points for R_p and are represented in Fig. 1 as • on the left-hand side of the figure. By setting gates in the $n\gamma\gamma$ matrix, we found five new γ-ray cascades. Figure 1 shows the values of R_p for the three strongest sequences, depending on the transition energies; the large symbols on the right-hand side of the figure (⋆, ■, and ∗) reflect the weighted mean of R_p within each cascade. As indicated by the dotted lines, the three sequences are consistent with $2p$, $3p$, and $4p$ evaporation, respectively. After that, we compared the ratios R_n and R_{2n} of the unknown cascades to the corresponding calibration values originating from ^{87}Mo, which is the only known [15] neutron reaction channel with a sufficient cross section. As a result, the three cascades were found to have neutron multiplicity one [17], whereas the other

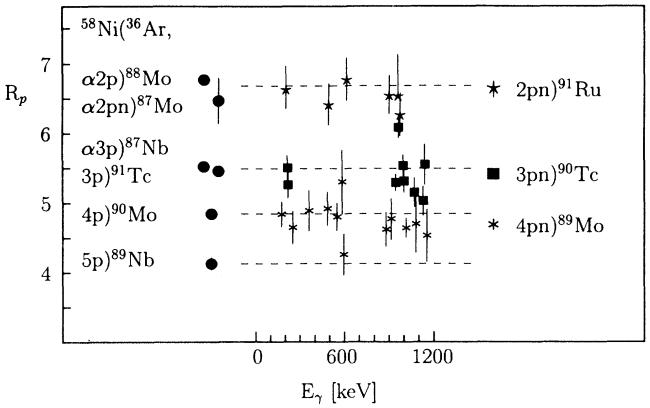

FIG. 1. Ratio of yields without and with one proton gating condition for some cascades. See text for details.

two sequences, which were not included in Fig. 1 yield a distinct enhancement of the $2n$ yields. Therefore assignments to ^{58}Ni(^{36}Ar,$3p2n$)^{89}Tc and ^{58}Ni(^{36}Ar,$2p2n$)^{90}Ru could be made for these two sequences [20]. None of the cascades in Fig. 1 were observed in the α-gated matrix and, hence, they can be unambiguously assigned to ^{58}Ni(^{36}Ar,$2pn$)^{91}Ru, ^{58}Ni(^{36}Ar,$3pn$)^{90}Tc, and ^{58}Ni(^{36}Ar,$4pn$)^{89}Mo.

Neutron gated $\gamma\gamma$ coincidences, intensities, and summed energy relationships were used to locate the various transitions in the ^{90}Tc level scheme. The level energies E_x and the connecting γ rays E_γ can be found in the left-hand side of Table I. The E_γ values given are the weighted means of several peak fits to different spectra. The level energies were calculated by performing an overall least-squares fit to all placed γ-ray transitions with the computer code LEFIT [30]. The intensities given in Table I are calculated relative to the 994-keV transition and reflect mean values evaluated from matched yields in either the $n\gamma\gamma$ projection or clean spectra. Intensities of transitions with $E_\gamma \leq 400$ keV were corrected for timing effects as described in [18].

Four γ-ray spectra taken under different gating conditions are displayed in Fig. 2: Fig. 2(a) is an $n\gamma\gamma$-spectrum gated on the 218-keV $13^- \rightarrow 12^-$ transition illustrating the negative parity band. In Fig. 2(b) the radiation summed over all 12 OSIRIS detectors was gated with an evaporated neutron. This spectrum shows that ^{90}Tc is the strongest neutron evaporation channel. Figure 2(c) displays the positive parity side with an $n\gamma\gamma$-spectrum gated on the 216-keV $15^+ \rightarrow 14^+$ transition. The last spectrum is a gate on the 462-keV transition depopulating the 9805-keV state. Despite its position at the top of the level scheme and hence, low relative intensity, one can detect even the coincident high energy γ rays at 1442, 1663, 1722, and 2301 keV. Furthermore, this cut illustrates the efficiency of the neutron gating leading to a background level near zero.

Apart from the possibilities of identifying new isotopes and constructing their level schemes this experiment yielded information on lifetimes via Doppler-shift attenuation line-shape analysis. For example, the slight broadening of the 430-, 462-, 804-, and 1288-keV lines

TABLE I. Excitation energy, transition energy, angular distribution coefficients, DCO ratios, and spin assignments.

E_x [keV]	E_γ [keV]	I_{rel} at 65°	A_2	A_4	δ	R_{DCO}	Gate[a]	Multi-polarity	$I_i^\pi \rightarrow I_f^\pi$[b]
152.6(3)	48.8(1)								$4^- \rightarrow [6^+]$
340.4(2)	187.8(1)	51(6)	-0.55(2)	0.05(3)	$0.23(^{7}_{6})$	$\ll 1$	F	$E2/M1$	$5^- \rightarrow 4^-$
	236.8(3)	5(3)							$5^- \rightarrow [6^+]$
494.1(1)	494.1(1)	130(5)	-0.60(4)	0.16(5)	$0.20(^{6}_{5})$	0.40(14)	B	$E2/M1$	$9^+ \rightarrow 8^+$
993.7(1)	499.7(1)	55(3)	-0.59(6)	-0.04(8)	0.3(2)	$\ll 1$	B	$E2/M1$	$10^+ \rightarrow 9^+$
	993.7(1)	1000(31)	0.31(2)	-0.06(2)		1.02(7)	B	$E2$	$10^+ \rightarrow 8^+$
1023.9(2)	683.5(1)	53(3)	0.31(8)	-0.03(8)		1.07(13)	F	$E2$	$7^- \rightarrow 5^-$
1485.9(1)	492.1(1)	139(5)	-0.51(3)	0.10(3)	0.15(4)	0.50(7)	A	$E2/M1$	$11^+ \rightarrow 10^+$
	991.5(2)	14(3)							$11^+ \rightarrow 9^+$
1613.9(1)	620.2(4)	7(2)							$[10_2^+] \rightarrow 10^+$
	1119.8(1)	33(2)							$[10_2^+] \rightarrow 9^+$
1632.0(1)	608.1(1)	53(5)	0.28(6)	-0.02(6)		0.82(18)	E	$E2$	$9^- \rightarrow 7^-$
	1137.8(3)	24(6)							$9^- \rightarrow 9^+$
1698.8(2)	1204.4(4)	9(3)							$[10_3^+] \rightarrow 9^+$
1938.6(1)	452.6(1)	32(2)	-0.35(14)	-0.09(16)				$E2/M1$	$12^+ \rightarrow 11^+$
	944.9(1)	554(17)	0.30(3)	-0.08(3)		0.95(6)	A	$E2$	$12^+ \rightarrow 10^+$
1995.1(1)	296.3(1)	7(3)							$11^- \rightarrow [10_3^+]$
	363.3(1)	26(6)				1.12(9)	F	$E2$	$11^- \rightarrow 9^-$
	381.3(1)	21(4)							$11^- \rightarrow [10_2^+]$
	509.1(1)	97(9)	0.38(8)	0.05(9)	$-0.05(^{59}_{87})$	1.10(23)	A	$E1$	$11^- \rightarrow 11^+$
	1001.4(1)	423(14)	-0.36(3)	0.08(3)	0.06(6)	0.59(6)	A	$E1$	$11^- \rightarrow 10^+$
2186.5(1)	191.6(1)	49(3)	0.31(4)	-0.01(4)	$0.2(^{3}_{10})$	1.13(12)	A	$E2/M1$	$11_2^- \rightarrow 11^-$
	554.4(1)	33(1)				0.85(7)	F	$E2$	$11_2^- \rightarrow 9^-$
	1192.8(5)	7(3)							$11_2^- \rightarrow 10^+$
2248.0(2)	309.5(2)	9(2)							$[12_2^+] \rightarrow 12^+$
2537.4(1)	598.9(1)	182(6)	-0.37(4)	0.08(4)	$0.07(^{10}_{8})$	0.53(7)	A	$E2/M1$	$13^+ \rightarrow 12^+$
	1051.5(1)	29(2)							$13^+ \rightarrow 11^+$
2557.9(1)	371.4(1)	24(2)							$12^- \rightarrow 11_2^-$
	562.8(1)	295(9)	-0.35(2)	-0.01(2)	0.08(3)	0.47(7)	A	$E2/M1$	$12^- \rightarrow 11^-$
2600.5(1)	413.9(1)	34(3)				$\ll 1$	A	$E2/M1$	$12_2^- \rightarrow 11_2^-$
	605.2(1)	57(3)				0.64(12)	A	$E2/M1$	$12_2^- \rightarrow 11^-$
2775.7(1)	175.0(1)	45(5)	c			$\ll 1$	A	$E2/M1$	$13^- \rightarrow 12_2^-$
	217.7(1)	258(10)	-0.33(2)	0.02(2)	0.06(3)	0.35(7)	A	$E2/M1$	$13^- \rightarrow 12^-$
	589.3(1)	19(3)							$13^- \rightarrow 11_2^-$
	780.6(1)	103(4)	0.39(6)	-0.09(6)		0.92(15)	D	$E2$	$13^- \rightarrow 11^-$
	837.1(1)	41(2)				0.43(17)	A	$E1$	$13^- \rightarrow 12^+$
2946.8(1)	409.4(1)	14(1)							$13_2^+ \rightarrow 13^+$
	698.9(2)	7(2)							$13_2^+ \rightarrow [12_2^+]$
	1008.5(2)	19(4)							$13_2^+ \rightarrow 12^+$
2982.1(1)	381.3(1)	16(3)							$[13_2^-] \rightarrow 12_2^-$
	424.2(1)	65(6)	c						$[13_2^-] \rightarrow 12^-$
3167.8(1)	221.2(1)	27(2)	-0.52(11)	0.19(14)		$\ll 1$	A	$E2/M1$	$14^+ \rightarrow 13_2^+$
	630.4(1)	26(3)				0.44(13)	A	$E2/M1$	$14^+ \rightarrow 13^+$
	1229.0(1)	288(10)	0.31(3)	-0.01(4)		1.00(8)	A	$E2$	$14^+ \rightarrow 12^+$
3201.2(1)	600.9(2)	24(5)							$[13_3^-] \rightarrow 12_2^-$
3383.3(1)	215.5(1)	249(10)	-0.27(2)	0.08(3)	$0.00(^{6}_{5})$	0.37(6)	C	$E2/M1$	$15^+ \rightarrow 14^+$
	845.8(1)	119(5)	c			1.15(12)	B	$E2$	$15^+ \rightarrow 13^+$
3405.8(1)	238.1(2)	5(2)							$[14_2^+] \rightarrow 14^+$
	868.4(2)	19(4)							$[14_2^+] \rightarrow 13^+$
3488.7(1)	287.5(1)	19(2)							$14^- \rightarrow [13_3^-]$
	506.5(1)	43(5)							$14^- \rightarrow [13_2^-]$
	713.1(1)	87(3)	-0.50(4)	0.10(4)	$0.14(^{9}_{6})$	0.39(10)	E	$E2/M1$	$14^- \rightarrow 13^-$
	930.6(2)	29(2)				0.76(18)	E	$E2$	$14^- \rightarrow 12^-$
3593.1(1)	187.4(1)	34(3)							$15_2^+ \rightarrow [14_2^+]$
	210.1(4)	9(4)							$15_2^+ \rightarrow 15^+$
	425.3(1)	83(3)	c			0.62(7)	C	$E2/M1$	$15_2^+ \rightarrow 14^+$
3673.0(1)	184.2(1)	175(7)	c			0.37(9)	E	$E2/M1$	$15^- \rightarrow 14^-$
	505.0(2)	20(4)							$15^- \rightarrow 14^+$
	897.4(1)	402(14)	0.34(3)	-0.05(3)		0.99(19)	A	$E2$	$15^- \rightarrow 13^-$
4486.6(2)	1103.0(1)	17(2)							$[16^+] \rightarrow 15^+$
4512.2(1)	919.1(1)	77(3)	0.30(12)	0.08(13)		1.28(11)	C	$E2$	$17^+ \rightarrow 15_2^+$
	1128.8(1)	240(8)	d			0.98(9)	C	$E2$	$17^+ \rightarrow 15^+$
4637.2(2)	964.2(1)	443(14)	0.30(2)	-0.10(2)		1.02(7)	D	$E2$	$17^- \rightarrow 15^-$
4864.9(2)	378.1(1)	10(2)							$[17_2^+] \rightarrow [16^+]$
	1481.9(2)	23(2)							$[17_2^+] \rightarrow 15^+$
5599.2(2)	1087.1(1)	22(2)							$[18^+] \rightarrow 17^+$
5651.3(2)	1139.1(1)	200(7)	0.25(4)	-0.03(5)		0.96(10)	C	$E2$	$19^+ \rightarrow 17^+$
5706.0(2)	1068.8(1)	286(9)	0.34(3)	-0.08(4)		1.02(10)	D	$E2$	$19^- \rightarrow 17^-$
5808.3(2)	209.2(2)	20(4)							$[19_2^+] \rightarrow [18^+]$
6338.7(2)	1473.8(2)	19(2)							$[19_3^+] \rightarrow [17_2^+]$

TABLE I. (*Continued*).

E_x [keV]	E_γ [keV]	I_{rel} at 65°	A_2	A_4	δ	R_{DCO}	Gate[a]	Multi-polarity	$I_i^\pi \rightarrow I_f^\pi$[b]
6455.3(2)	647.1(1)	17(2)							$(20^+) \rightarrow [19_2^+]$
	803.9(2)	138(6)	e			0.52(18)	S	$(E2/M1)$	$(20^+) \rightarrow 19^+$
6884.9(2)	429.6(1)	39(4)				0.73(10)	C	$(E2/M1)$	$(21^+) \rightarrow (20^+)$
6994.0(2)	1288.0(1)	169(6)	0.27(4)	-0.04(4)	e	0.87(14)	D	$E2$	$21^- \rightarrow 19^-$
7373.5(3)	1722.2(5)	11(3)							$[20_2^+] \rightarrow 19^+$
7439.7(4)	445.7(3)	40(2)	e						$[22^-] \rightarrow 21^-$
7678.9(3)	305.4(2)	8(2)							$[21_2^+] \rightarrow [20_2^+]$
	1340.2(2)	15(1)							$[21_2^+] \rightarrow [19_3^+]$
8394.5(4)	954.8(2)	28(3)	c,e						$[23^-] \rightarrow [22^-]$
8757.0(3)	1077.8(5)	5(2)							$[22^+] \rightarrow [21_2^+]$
	1872.2(3)	12(3)							$[22^+] \rightarrow (21^+)$
	2300.8(3)	10(2)							$[22^+] \rightarrow (20^+)$
9342.4(4)	585.7(2)	33(4)				0.73(14)	C	$(E2/M1)$	$(23^+) \rightarrow [22^+]$
	1663.0(4)	10(2)							$(23^+) \rightarrow [21_2^+]$
9804.5(5)	462.1(1)	36(4)				0.65(14)	A	$(E2/M1)$	$(24^+) \rightarrow (23^+)$
11246.7(7)	1442.2(2)	23(4)				1.05(21)	S	$(E2)$	$(26^+) \rightarrow (24^+)$

[a] A: 994 keV, B: 945 keV, C: 1229 keV, D: 897 keV, E: 964 keV, F: 608 keV, S: sum of 994, 945, 1229, 846, 1129, and 1139 keV.

[b] Square brackets reflect spin assignments proposed by theory and yrast arguments.

[c] Doublet structure with transitions from ^{89}Mo.

[d] Doublet structure with a transition from ^{90}Mo β-decay.

[e] DSA line shape.

in Figs. 2(a) and 2(c) and the broad distribution of the 446-keV line in Fig. 2(a) are indications of short lifetimes below some few picoseconds. Furthermore, directional correlation of oriented states (DCO) ratios here defined as

$$R_{DCO} := \frac{I(\gamma_1 \text{ at } 162°;\ \text{gated with } \gamma_2 \text{ at } 65°, 115°)}{I(\gamma_1 \text{ at } 65°, 115°\ ;\ \text{gated with } \gamma_2 \text{ at } 162°)} \quad (1)$$

have been evaluated to suggest the multipole characters of the transitions. The intensities have been corrected for the efficiency of both observing and gating detector. About 4×10^7 events were sorted in the DCO-$\gamma\gamma$ matrix. Only $E2$ transitions were used as gates. Some 40 DCO ratios are given in Table I together with the adjacent gate. The expected values are R_{DCO}=1.0 for a stretched $E2$ transition and $R_{DCO} \approx 0.5$ for a stretched $\Delta I = 1$ transition.

B. Angular distributions

An angular distribution experiment was carried out at the Van de Graaff tandem accelerator in Cologne in order to make spin parity assignments. The reaction ^{58}Ni(^{35}Cl,2pn)^{90}Tc was used at 120 MeV beam energy. The target was a 99.98% enriched 16.3 mg/cm^2 thick ^{58}Ni foil. As no ns isomers were found in ^{90}Tc in the experiment described above, possible attenuations of the angular momentum alignment due to the internal ferro-

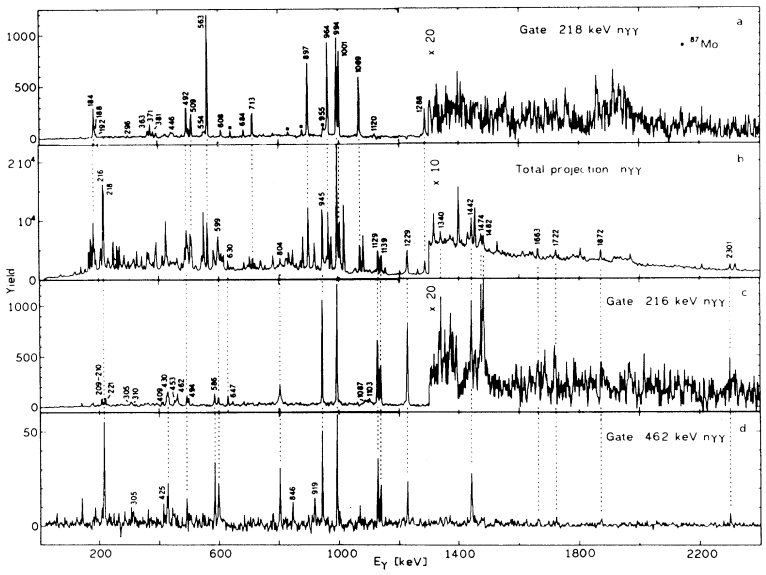

FIG. 2. Prompt $n\gamma\gamma$ spectrum from the ^{58}Ni + ^{36}Ar reaction (b) and $n\gamma\gamma$ coincidence spectra in the OSIRIS spectrometer with gates set on ^{90}Tc lines: (a) 218 keV $13^- \rightarrow 12^-$ transition, negative parity side; (c) 216 keV $15^+ \rightarrow 14^+$ transition, positive parity side; (d) 462 keV $(24^+) \rightarrow (23^+)$ transition, π=+ high spin region. The numbers given in the spectra are the peak energies in keV.

magnetic field were neglected. Four Ge detectors were used to detect the γ radiation. They had relative efficiencies of 25–55 % and energy resolutions of 1.9–2.1 keV at E_γ=1.3 MeV. One detector was fixed at 125° relative to the beam to monitor the beam current. The other detectors (D1–3) were mounted with relative angles of 55° and 45° to each other, scanning the regions from −90° to +10° (D1), −35° to +65° (D2), and +10° to +110° (D3). In addition, two large volume NE213 neutron detectors were located 5.5 cm below and above the beam spot in order to take the γ-ray angular distribution in the $1n$-gating mode. Furthermore, a planar Ge detector was used as a low energy photon spectrometer (LEPS). This detector was mounted at 142° and operated within the energy range 20–150 keV and in coincidence with the four Ge detectors and the neutron detectors. LEPS calibration was done with a ^{241}Am source.

Corrections of the intensities of the individual γ rays were performed firstly for the beam current with γ-ray yields measured in the monitor detector and, secondly, for ADC dead-time effects. The three movable detectors run at rates of approximately 10^4 counts leading to ADC dead times of about 30%. In case of the fixed detector these values were reduced by a factor of 3 due to the smaller solid angle. A possible asymmetry of the chamber and angle dependent γ-ray absorption were checked with spectra from long-living activities and ^{152}Eu and ^{133}Ba sources and by comparing the yields of transitions from reaction products at −35° and +35° in detector D2. The mean of the ratio $I(+35°)/I(-35°)$ amounts to 0.99(1). No asymmetry was observed with the activity and calibration spectra. Only at one position an enhanced absorption was found for $E_\gamma \leq$150 keV due to the target frame. Subsequently, the intensities in the three movable detectors were matched to each other. This procedure yielded data points at 12 different angles between 0° and 90°. The left and middle parts of Fig. 3 show some examples of least-squares fits to the data using the Legendre polynomial formula [31]

$$W(\Theta) = A_0 + A_2 P_2(\cos\Theta) + A_4 P_4(\cos\Theta). \qquad (2)$$

These fits were deduced from two angular distribution least-squares computer codes named AD [32] and CHIPLO [33]. The A_2 and A_4 values listed in the middle of Table I are the fitted numbers corrected for the attenuation due to finite solid angles of the Ge detectors [34]. Mixing ratios $\delta(E2/M1)$ were evaluated for 12 transitions in the phase convention of Rose and Brink [35]. The determination of δ strongly depends on the alignment factor σ, which describes the width of the magnetic substate distribution assumed to be Gaussian. The σ values can be determined from the attenuation coefficients defined by $\alpha_k := A_k(\text{exp})/A_k(\text{theo})$, $k = 2, 4$ of stretched $E2$ transitions and can be inferred into the alignment of subsequent states using the U_k coefficients and the feeding pattern, always on condition of fast transitions. In our case σ was found to be 4.4(5) at $I = 19\hbar$ deduced from the fits to the data of the 964-, 1069-, and 1139-keV transitions. This results in σ=3.1(3) for the 994-keV $10^+ \rightarrow 8^+$ transition which is in excellent agreement with its fitted value σ=3.2(3). The χ^2 analysis [36] of several transitions is illustrated in the right part of Fig. 3. The full curves correspond to the analysis with the calculated σ or α_2/α_4 values. The dashed ones represent their upper and lower limits. The resulting mixing ratios given in Table I refer to the absolute minima of the first curves with the errors extracted from the crossing points of the latter with the 0.1% confidence limit. Only the minima with $\delta \approx 0$ were considered, since large $E2$ admixtures to $\Delta I = 0$ or $\Delta I = 1$ transitions ($\delta \rightarrow \infty$) are unlikely due to the similarities of the wave functions of the adjacent states (see Sec. IV). The change in parity was marked with the mixing ratio of the 1001-keV $11^- \rightarrow 10^+$ transition, which is consistent with zero. If it was a mixed $E2/M1$ transition the mixing ratio should be distinctly different from zero due to its large transition energy. For example, the mixing ratio of the 713-keV $14^- \rightarrow 13^-$ transition amounts to δ=0.39(10). The DCO ratios were consistent with the results of the angular distribution measurement and even the mixing ratios deduced from the DCO ratios and angular distributions are in very good agreement [37]. Therefore the DCO ratios allowed us to assign multipolarities to some 20 more transitions. Spin parity assignments are given on the right-hand side of Table I. Values in square brackets are suggestions arising from theory, which will be discussed later on.

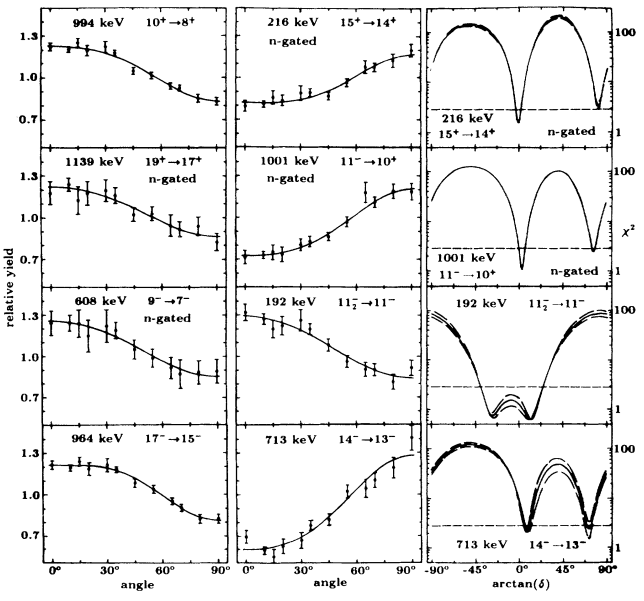

FIG. 3. Angular distributions and χ^2 analysis of the mixing ratio δ for adjacent ΔI=1 transitions in ^{90}Tc. The lines through the data points are least squares fits to the angular distribution formula (2). The full curves in the χ^2 plots correspond to the analysis with the calculated width σ of the magnetic substate distribution. The dashed ones represent calculations with the upper and lower limits of σ.

III. THE LEVEL SCHEME OF ^{90}Tc

A. The ^{90}Tc ground state

The level scheme based on the experiments described in the preceding section is presented in Fig. 4. The first quantity to discuss in case of an odd-odd nucleus is its ground-state spin. Oxorn *et al.* [25] found two β-unstable states in ^{90}Tc and assigned spins of (6^+) to the 49.2(4)s ^{90m}Tc level and 1^+ to the 8.7(2)s ^{90g}Tc level. Both decays should have approximately the same Q value. Nevertheless, we claim the lowest state observed in our investigation to have $I^\pi=8^+$ and the 994-keV γ ray to be the $10^+ \rightarrow 8^+$ yrast transition. The first arguments are based on systematics: All neighboring odd-odd $N = 47, 49$ nuclei ^{88,90}Nb [38, 39] and ^{92}Tc [40] have a definite ground-state spin of $I^\pi=8^+$ measured either by β-decay or transfer reactions. In ^{86}Y, the lowest positive parity state was found also to have $I^\pi=8^+$ [22]. The $10^+ \rightarrow 8^+$ transition energies in the ^{90}Tc isotones ^{86}Y and ^{88}Nb are 1107 keV [22] and 1089 keV [10], close in energy to the 994-keV transition. Moving toward the $N = 45$ odd-odd nuclei, the 6^+ state becomes lower in energy as observed in ^{84}Y [41]. The situation seems to be similar in ^{86}Nb [9, 11] and ^{88}Tc [19]. Yet the γ-ray energies connecting the 8^+ and 6^+ states are about 300 keV and all the 8^+ states have probably isomeric character [41]. The energies of the $10^+ \rightarrow 8^+$ transitions again are about 900 keV in these nuclei.

The second argument arises from results of the LEPS-γ coincidences in combination with the predictions of the shell model calculations: Comparing the ungated and neutron gated LEPS-single spectra, a so-far unknown 49-keV line was found to belong to a neutron evaporation channel. A gate set on this transition in the LEPS-γ matrix revealed weak coincidences with the 188-, 684-, and 608-keV transitions in ^{90}Tc built upon the 153-keV 4^- state. A distinct coincidence between the 49- and 188-keV transitions was observed in the $\gamma\gamma$ matrix. However, statistics were too poor to observe clear coincidences between the 49-keV transition and the 684- and 608-keV transitions, respectively. Nevertheless, a 237-keV transition is observed in the $n\gamma\gamma$ and $\gamma\gamma$ data, possibly a decay of the 340-keV 5^- state. This leads to the level at 104 keV with a possible spin $I^\pi=6^+$. We note that the 6^+ state with a $\tau=88$ μs lifetime in ^{90}Nb lies 123 keV above the 8^+ ground state [42], while in ^{92}Tc the difference amounts to 214 keV [43]. The shell model calculation for ^{90}Tc (see below) predicts the ground-state spin to be $I^\pi=8^+$. Other predicted low-lying levels are the 2^+ (143 keV), 4^- (340 keV), and 6^+ (106 keV) state. The theoretical results reproduce the experimental states only if one matches the lowest experimentally observed state to the calculated 8^+ ground state. Moreover, the theoretical difference of 106 keV between the excited 6^+ state and the 8^+ ground state fits very well to the 104-keV level distance discussed above. A measurement focused on the low excitation region in ^{90}Tc should clarify the situation.

B. Negative parity states

Above the 994-keV 10^+ state the γ-ray flux divides in two branches—the 945-keV transition continues the positive parity structure, the 1001-keV transition transports most of the flux from the negative parity states. The second strong path from these states is the 509–492-keV $11^- \rightarrow 11^+ \rightarrow 10^+$ sequence. Both the 509- and 1001-keV transitions have mixing ratios consistent with zero. The 563–218–713–184-keV cascade of four stretched dipole transitions is built upon the 1995-keV 11^- state. They are accompanied by the comparatively weak 781-keV $13^- \rightarrow 11^-$ and 931-keV $14^- \rightarrow 12^-$ transitions and the strong 897-keV $15^- \rightarrow 13^-$ γ ray. At higher excitation energies even spins were not observed and the band continues by a cascade of three stretched quadrupole transitions up to spin $I^\pi=21^-$ at the 6994-keV state. The negative parity ends with two γ rays at 446 and 955 keV. In addition, a weak decay branch depopulating the 1995-keV 11^- and 2187-keV 11_2^- states down to the 153-keV 4^- level was established. Several transitions connecting yrast and yrare states in the $I=(11\text{–}15)\hbar$ spin region were found. Several other possible parity changing transitions

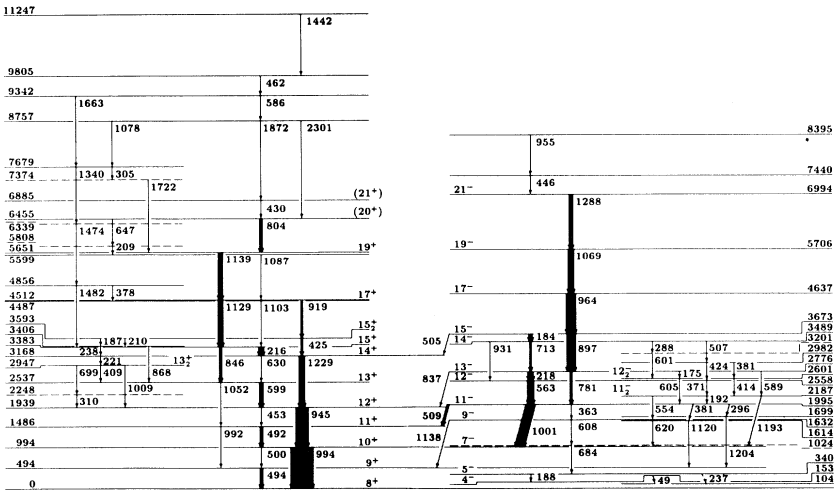

FIG. 4. Level scheme of ^{90}Tc deduced from the present work. The width of the arrows connecting the levels are proportional to the relative γ-ray intensities. If the intensities of the feeding and the depopulating transition are equal within their errors, the corresponding levels are dotted. In these cases populating and depopulating γ rays might be inverted changing the level energy. Energies are given in keV.

were observed, but due to low statistics no angular distribution coefficients could be extracted.

C. Positive parity states

Switching to the positive parity states, many transitions and yrare levels were observed in the I=(11–15)$\hbar$ spin window. The main γ-ray flux, however, splits up at the 1939-keV 12^+ state into the two sequences 599–846 keV and 1229-216 keV and then once more at the 3168-keV 14^+ state into two 15^+ states via the 216–1129-keV and 425–919-keV cascades. Then the 4512-keV 17^+ and the 5651-keV 19^+ levels collect the flux again. Spin assignments are straightforward for all these levels. For the following two transitions of 804 and 430 keV only DCO ratios were evaluated, which suggest ΔI=1 character for both transitions. Thus tentative spin assignments of (20^+) and (21^+) to the 6455- and 6885-keV levels are given. At the top of the level scheme an ensemble of another eight transitions was arranged. Despite the comparatively weak intensities of these transitions the low background level of the $n\gamma\gamma$ matrix allowed us to observe coincidences even between themselves [see Fig. 2(d)]. Furthermore, summed energy relations ensure the placement of the 7679-, 8757-, and 9342-keV levels. The succession of the 462- and 1442-keV transitions at the top of the level scheme was chosen on the basis of their relative intensities. The DCO ratios of the 462- and 586-keV transitions are consistent with stretched dipole character, whereas the 1442-keV transition is most probably a stretched quadrupole.

IV. DISCUSSION

A. $N = 47$ and $Z = 43$ systematics

As ^{90}Tc reveals a complex irregular high spin excitation scheme an interpretation based on the shell model is favored. Before discussing the shell model interpretation of ^{90}Tc in more detail, we shall present it in an illustrative way by comparing it to neighboring isotopes. Figure 5 displays the ^{90}Tc positive parity $I \leq 15$ states and the levels of the $N = 47$ odd-odd isotones ^{88}Nb [10] and ^{92}Tc [43]. The two ^{88}Nb levels fit well to the yrast states in ^{90}Tc, whereas those of ^{92}Tc have a larger level spacing up to I=12$\hbar$. In calculations performed by Oxorn *et al.* [10] the first excited 10^+ and 12^+ states in ^{88}Nb are proposed to have $\pi(g_{9/2})^1\nu(g_{9/2})^{-3}_{13/2}$ and $\pi(g_{9/2})^1\nu(g_{9/2})^{-3}_{17/2}$ configurations, respectively. In contrast, ^{92}Tc possesses only one neutron hole with respect to the $N = 50$ shell closure, thus a broken $g_{9/2}$ proton pair must be used to increase spin. Accordingly, the wave functions of the low-lying ^{92}Tc states are proposed to have $\pi(g_{9/2})^3_i\nu(g_{9/2})^{-1}$, i=13/2,17/2,21/2 configurations [43].

In Fig. 6 the main positive and negative parity sequences of ^{90}Tc are compared to those in the odd-A neighbors ^{89}Mo ($N = 47$) and ^{89,91}Tc ($Z = 43$). The data on these nuclei were taken from [17, 20, 44]; the extension of the ^{91}Tc levels above I^π=35/2$^+$ as well as the decay branch down to the I^π=1/2$^-$ level was also

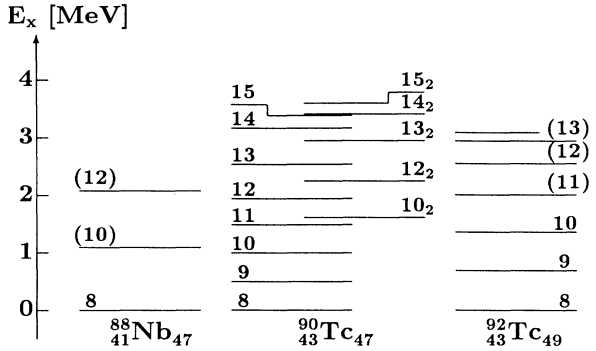

FIG. 5. Positive parity energy level systematics with odd-odd neighbors. The yrast and yrare levels up to $I = 15\hbar$ in ^{90}Tc are compared to levels in the isotone ^{88}Nb [10] and the isotope ^{92}Tc [43].

evaluated from our OSIRIS experiment. On the positive parity side, the level spacings are very similar, apart from the low spin sequence in ^{89}Tc, where the $21/2^+ \rightarrow 17/2^+$ transition energy (695 keV) is larger as compared to ^{91}Tc (316 keV) and ^{89}Mo (487 keV).

Several authors suggested that vibrational excitations occur in the low spin region of $N = 48$ nuclei [23, 10] because the experimentally observed 2^+, 4^+ and $13/2^+$, $17/2^+$ energy levels do not correspond to the shell model predictions. These calculations were performed within a $p_{1/2}$-$g_{9/2}$ configuration space for both protons and neutrons and a charge independent effective interaction [23]. Indications of vibrational contributions may also be seen in the ^{90}Tc level scheme: The 994-keV $10^+ \rightarrow 8^+$ and the 945-keV $12^+ \rightarrow 10^+$ transitions have similar energies. There is also a distinct staggering of the branching ratios b of the four mixed ΔI=1 transitions in the I^π=8$^+$–12$^+$ range: $b(12^+ \rightarrow 11^+) = 0.047(5) \approx b(10^+ \rightarrow 9^+) = 0.043(2)$ but $b(11^+ \rightarrow 10^+)$=0.89(5) $\approx b(9^+ \rightarrow 8^+)$=1.0. This staggering of intensities directly transforms into a staggering of the transition strength

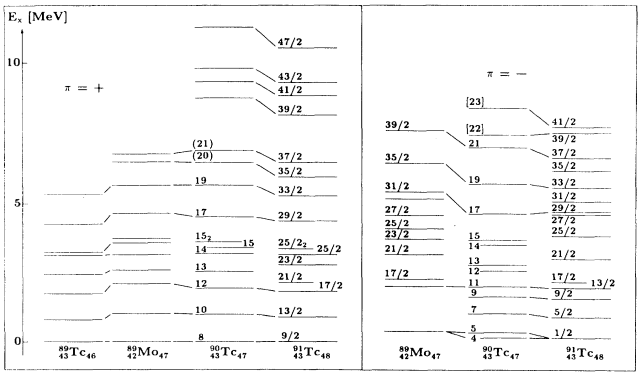

FIG. 6. $N = 47$ and $Z = 43$ energy level systematics with odd-A neighbors. The level scheme of ^{90}Tc is compared to the level schemes of ^{89,91}Tc [20, 44] and ^{89}Mo [17]. Levels, which are supposed to correspond to each other, are connected with lines.

because all of these transitions have similar mixing ratios $\delta \approx 0.2$–0.3 and γ-ray energies. This pattern may be associated with contributions arising from one and two phonon excitations but clearly lifetimes are necessary to clarify the situation. The states in the intermediate spin regime $I=(13$–$15)\hbar$ seem to fit well into the energy systematics but they cannot be associated with states in the neighboring odd-A isotopes because proton and neutron-hole excitations compete with each other in that spin region. In ^{89}Mo a broken proton pair couples to the unpaired neutron, in ^{91}Tc a broken neutron-hole pair couples to the unpaired proton. To gain spin larger than $I = 15\hbar$ in ^{90}Tc or $I = 25/2\hbar$ in the other nuclei proton *and* neutron excitations are necessary if only $2p_{1/2}$ and $1g_{9/2}$ orbits for either protons or neutrons were considered.

The interpretation of the negative parity levels is less evident. Apart from similar difficulties in the intermediate spin range, the odd-A neighbors reveal $\Delta I=1$ staggering even at high spins. However, the $E2$ cascade depopulating the $39/2^-$ state [55% $\pi(p_{1/2})^1\pi(g_{9/2})^3_{21/2}\nu(g_{9/2})^{-3}_{17/2}$ and 43% $\pi(p_{1/2})^1\pi(g_{9/2})^3_{17/2}\nu(g_{9/2})^{-3}_{21/2}$] in ^{89}Mo may be associated with the $21^- \rightarrow 19^- \rightarrow 17^-$ sequence in ^{90}Tc. By adding a neutron hole to the $\pi(p_{1/2})^1\pi(g_{9/2})^4_{12}\nu(g_{9/2})^{-2}_8$ $41/2^-$ state in ^{91}Tc one ends up with a possible level with $I^\pi=23^-$ in ^{90}Tc. If we attribute this spin to the 8395-keV level the previously mentioned $E2$ cascade should coincide with the $37/2^-$, $33/2^-$, and $29/2^-$ levels in ^{91}Tc. The level spacings of both nuclei are in reasonable agreement, but their decay patterns are rather different: ^{90}Tc deexcites via stretched $E2$ transitions, whereas ^{91}Tc has strong $\Delta I=1$ decay branches. In the low spin part of their level schemes the similarities between the Tc isotopes are again striking. The additional $g_{9/2}$ neutron hole couples to the $p_{1/2}$ proton to spins $I^\pi=4^-$ or 5^-, thereafter a $\nu(g_{9/2})^{-2}_{2,4,6}$ neutron hole pair leads to a $\Delta I=2$ sequence up to spin $I^\pi=11^-$.

B. The shell model interpretation

The configuration space utilized in our calculation consists of only the $2p_{1/2}$ and $1g_{9/2}$ orbitals for protons and neutrons. According to that, ^{90}Tc has five valence protons and three neutron holes with respect to the ^{88}Sr core with the subshell closures at $Z = 38$ and $N = 50$ commonly used in this mass region [23, 45, 46]. The calculations in the present study were performed in a convenient proton-neutron particle-particle formalism with the computer code RITSSCHIL [47]. The two-body matrix elements of the residual interaction and the four single-particle energies were taken from Gross and Frenkel [23] who deduced these parameters from a fit to energy levels of $N = 48$ and $N = 50$ nuclei under the condition of preserving charge independence of the nucleon-nucleon interaction. The eight valence particles/holes provide many coupling schemes up to spin $I = 23\hbar$, whereas experimental spin assignments in ^{90}Tc reach up to (21^+) and (23^-). Shell model calculations in ^{90}Mo by Kabadiyski *et al.* [18] were performed with a much larger configuration space including the proton orbits $1f_{5/2}$, $2p_{3/2}$, $2p_{1/2}$, and $1g_{9/2}$ and the neutron orbits $2p_{1/2}$, $1g_{9/2}$, $1g_{7/2}$, $2d_{5/2}$, $2d_{3/2}$, and $3s_{1/2}$. These authors found that excitations across the $N = 50$ shell gap do not contribute significantly to the wave functions of ^{90}Mo states. Moreover, excitations of $1f_{5/2}$ or $2p_{3/2}$ protons become important only at very high spins, for example, the yrast 20^+ state in ^{90}Mo consists mainly of a completely aligned $\pi(f_{5/2})^6\pi(p_{1/2})^0\pi(g_{9/2})^4_{12}\nu(g_{9/2})^{-2}_8$ configuration, whereas the yrare 20^+ or the yrast 21^+ states have $\pi(f_{5/2})^5\pi(p_{1/2})^1\pi(g_{9/2})^4_{12}\nu(g_{9/2})^{-2}_8$ character. Thus we found it sufficient to describe the states in ^{90}Tc within the restricted proton and neutron $1g_{9/2}$ $2p_{1/2}$ model space.

Figure 7 displays a comparison of the experimental and theoretical excitation schemes of ^{90}Tc. The theoretical levels are shifted slightly up in order to optimize the overall agreement between theory and experiment. This binding energy shift (BES) and the mean level deviation (MLD) are defined in [23]. In ^{90}Tc, the fit to 23 levels up to spin $I = 21\hbar$ results in a BES of only 50 keV and a MLD of only 100 keV. In the following the states

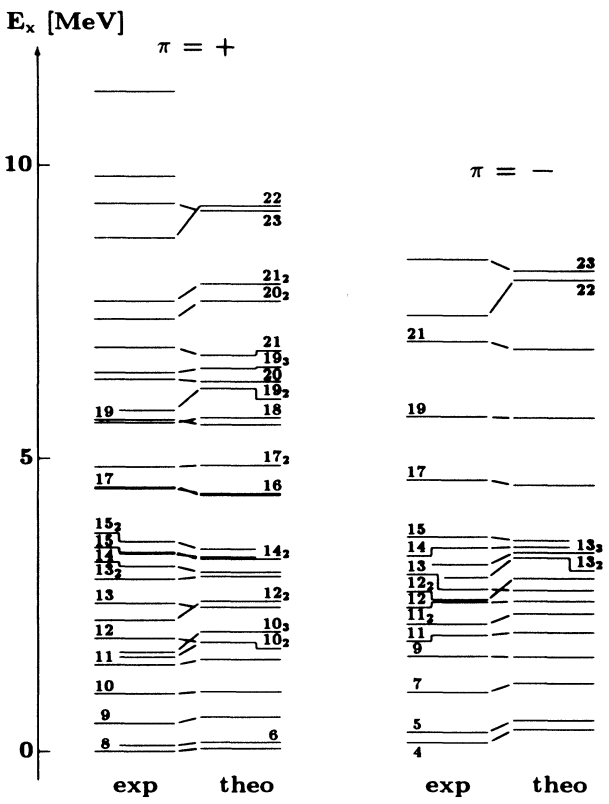

FIG. 7. Comparison of the experimental level scheme and the RITSSCHIL shell model calculation within the $p_{1/2}, g_{9/2}$ configuration space. If the spin was deduced from the experiment, it is denoted upon the experimental level. Otherwise the experimental levels are connected to the most probable theoretical levels.

with different parities are discussed in terms of increasing seniority $v = v_\pi + v_\nu$.

1. *Positive parity states*

The main components of the wave functions of certain positive parity states are shown in Table II in comparison to the states in the neighboring nuclei ^{91}Tc, ^{89}Mo, and ^{90}Mo, which is the nearest even-even core.

(*i*) v=2. The two $g_{9/2}$ particles can couple to spins $I = (0-9)\hbar$. According to the Nordheim rules in the spherical limit, the 8^+ state is predicted to be the lowest of the multiplet. Because of isospin repulsion, the odd spin states lie some hundred keV above those with even spins. The predicted $9^+ \rightarrow 8^+$ energy, 554 keV, is close to the experimentally observed 494 keV. The admixture of partitions with $v > 2$ to the 8^+ state is comparatively large (Table II) and this effect is even more pronounced for the 6^+ state, which has only 41% $\pi(g_{9/2})^1\nu(g_{9/2})^{-1}$ character. It is predicted at 106 keV excitation energy.

(*ii*) v=4. Completely aligned configurations with seniority $v = 4$ can reach up to spin $I = 15\hbar$; $\pi(g_{9/2})^1\nu(g_{9/2})^{-3}_{21/2}$ or $\pi(g_{9/2})^3_{21/2}\nu(g_{9/2})^{-1}$. Indeed, two closely lying 15^+ states are observed at 3383 and 3593 keV excitation energy. The theoretical energy separation is calculated to be 136 keV; the experimental value is 210 keV, similar to the 231 keV difference of the two $\pi(g_{9/2})^2_8$ and $\nu(g_{9/2})^{-2}_8$ 8^+ states in ^{90}Mo. The experimental decay branch from the 15^+_2 into the 15^+_1 state is very weak [b = 0.07(3)] also indicating a different nature of these states. The calculation predicts the $\pi(g_{9/2})^1\nu(g_{9/2})^{-3}_{21/2}$ configuration to be yrast. This is in agreement with g-factor measurements in the neighboring even-even nuclei ^{84}Sr [48], ^{86,88}Zr [49, 50], and ^{88,90}Mo [49, 50], which give evidence for a $\nu(g_{9/2})^{-2}_8$ configuration of the lowest 8^+ states. In our calculations the 8^+_1 state in ^{90}Mo has a 72% $\nu(g_{9/2})^{-2}_8$ contribution and only a 1.6% $\pi(g_{9/2})^2_8$ partition. The calculated wave functions of the $21/2^+$ and $25/2^+$ states in ^{91}Tc have mostly $\pi(g_{9/2})^1\nu(g_{9/2})^{-2}_8$ character and a negligible contribution of the $\pi(g_{9/2})^3_{21/2}$ configuration. Another neutron hole coupled to the main configurations leads to the $\pi(g_{9/2})^1\nu(g_{9/2})^{-3}_{21/2}$ state in ^{90}Tc, which is predicted to contain 56% of that partition. The 15^+_2 state [60% $\pi(g_{9/2})^3_{21/2}\nu(g_{9/2})^{-1}$, but 2.1% $\pi(g_{9/2})^1\nu(g_{9/2})^{-3}_{21/2}$] can be derived by first coupling a neutron hole to the 8^+_2 in ^{90}Mo [74% $\pi(g_{9/2})^2_8$, 1.4% $\nu(g_{9/2})^{-2}_8$] leading to either the $21/2^+$ [61% $\pi(g_{9/2})^2_8\nu(g_{9/2})^{-1}$, 1.0% $\nu(g_{9/2})^{-3}_{21/2}$] or $25/2^+$ [46% $\pi(g_{9/2})^2_8\nu(g_{9/2})^{-1}$] states in ^{89}Mo and then adding the $g_{9/2}$ proton to form the $\pi(g_{9/2})^3_{21/2}\nu(g_{9/2})^{-1}$ states in ^{90}Tc. The situation is similar for the two 14^+ and 13^+ states: The yrast states have essentially neutron hole excitation character $\pi(g_{9/2})^1\nu(g_{9/2})^{-3}_{21/2}$ the yrare

TABLE II. Wave functions of positve parity states in ^{89,90}Mo and ^{90,91}Tc.

Isotope	Spin [$\hbar$]	Wave function Ψ		Contribution [%]
^{90}Mo	0^+	$\pi(g_{9/2})^0$	$\nu(g_{9/2})^{-0}$	86.0
^{89}Mo	$9/2^+$		$\nu(g_{9/2})^{-1}$	74.2
^{91}Tc	$9/2^+$	$\pi(g_{9/2})^1$		76.7
^{90}Tc	8^+	$\pi(g_{9/2})^1$	$\nu(g_{9/2})^{-1}$	52.1
	9^+	$\pi(g_{9/2})^1$	$\nu(g_{9/2})^{-1}$	72.7
^{90}Mo	8^+		$\nu(g_{9/2})^{-2}_8$	71.9
		$\pi(g_{9/2})^2_8$		1.6
	8^+_2		$\nu(g_{9/2})^{-2}_8$	1.4
		$\pi(g_{9/2})^2_8$		74.1
^{89}Mo	$21/2^+$		$\nu(g_{9/2})^{-3}_{21/2}$	1.0
		$\pi(g_{9/2})^2_{6,8}$	$\nu(g_{9/2})^{-1}$	60.9
	$25/2^+$	$\pi(g_{9/2})^2_8$	$\nu(g_{9/2})^{-1}$	46.2
^{91}Tc	$21/2^+$	$\pi(g_{9/2})^1$	$\nu(g_{9/2})^{-2}_{6,8}$	59.1
		$\pi(g_{9/2})^3_{21/2}$		0.4
	$25/2^+$	$\pi(g_{9/2})^1$	$\nu(g_{9/2})^{-2}_8$	64.1
^{90}Tc	15^+	$\pi(g_{9/2})^1$	$\nu(g_{9/2})^{-3}_{21/2}$	55.6
		$\pi(g_{9/2})^3_{21/2}$	$\nu(g_{9/2})^{-1}$	0.5
	15^+_2	$\pi(g_{9/2})^1$	$\nu(g_{9/2})^{-3}_{21/2}$	2.1
		$\pi(g_{9/2})^3_{21/2}$	$\nu(g_{9/2})^{-1}$	60.0
^{90}Mo	16^+	$\pi(g_{9/2})^2_8$	$\nu(g_{9/2})^{-2}_8$	97.7
^{89}Mo	$37/2^+$	$\pi(g_{9/2})^2_8$	$\nu(g_{9/2})^{-3}_{21/2}$	93.6
^{91}Tc	$37/2^+$	$\pi(g_{9/2})^3_{21/2}$	$\nu(g_{9/2})^{-2}_8$	99.4
^{90}Tc	21^+	$\pi(g_{9/2})^3_{21/2}$	$\nu(g_{9/2})^{-3}_{21/2}$	97.6

states proton character $\pi(g_{9/2})^3_{21/2}\nu(g_{9/2})^{-1}$. The partitions of these states indicate that the $\pi(g_{9/2})^2$–$\nu(g_{9/2})^{-2}$ splitting effect becomes less important with decreasing spin. Accordingly, the states with $10 \leq I \leq 12$ are mixed.

(*iii*) v=6, $v_\pi = v_\nu$=3. These seniority $v = 6$ configurations extend the spins up to $I = 21\hbar$. An also possible v_π=5, v_ν=1 $\pi(g_{9/2})^5_{25/2}\nu(g_{9/2})^{-1}$ 17^+ contribution is of negligible amount. The 4512-keV 17^+_1 state is a mixture of three contributions: $\pi(g_{9/2})^3_{17/2}\nu(g_{9/2})^{-3}_{17/2}$ (29%), $\pi(g_{9/2})^3_{13/2}\nu(g_{9/2})^{-3}_{21/2}$ (25%), and $\pi(g_{9/2})^3_{21/2}\nu(g_{9/2})^{-3}_{13/2}$ (25%). Due to the predicted balanced partitions of the 17^+_1 state and the rather pure configurations of the 15^+ levels, the theoretical branching ratio should be given by $b_{\text{theo}}=(1129/919)^5=2.8$ if proton and neutron effective charges are similar. This is in good agreement with the experimental branching ratio b_{expt}=3.1(2). The 5651-keV 19^+_1 state consists of $\pi(g_{9/2})^3_{17/2}\nu(g_{9/2})^{-3}_{21/2}$ (47%) and $\pi(g_{9/2})^3_{21/2}\nu(g_{9/2})^{-3}_{17/2}$ (50%). The (19^+_2), (20^+_1), and (21^+_1) states are predicted to have almost pure aligned $v = 6$ $\pi(g_{9/2})^3\nu(g_{9/2})^{-3}$ configurations and almost no $v = 8$ partitions. This is supported by the experimental decay pattern: There is no $21^+_1 \rightarrow 19^+_1$ $E2$ transition observed, but two $M1$ transitions. These dipoles are supposed to be spin recoupling transitions within this $\pi(g_{9/2})^3\nu(g_{9/2})^{-3}$ seniority scheme. Moreover, a distinct feeding of the possible 5808 keV (19^+_2) state from the (20^+_1) is observed though hindered by energy. Again the wave functions can be understood in terms of adding a proton and neutron hole to ^{90}Mo.

(*iv*) $v \geq 8$. A completely aligned seniority $v = 8$ $\pi(g_{9/2})^5_{25/2}\nu(g_{9/2})^{-3}_{21/2}$ configuration provides two levels with $I = 22\hbar$ and $I = 23\hbar$ as well as yrare states with lower spins. The calculated excitation energies are near 9.2 MeV with the 23^+ state predicted 50 keV *below* the 22^+ level. Experimentally six levels above the 6885-keV (21^+_1) are observed. The two states near 7.5 MeV excitation energy are supposed to be the yrare (20^+_2) and (21^+_2) states having large $v = 8$ contributions in their wave functions. Furthermore, we attribute the two levels at 8757 keV and 9342 keV to the calculated 22^+ and 23^+ states though the energy difference of 586 keV is in contrast to the predicted 50-keV inversion. This assumption arises from the decay pattern of these levels; despite the branch into the yrast band there is also a decay observed into the yrare 7679 keV (21^+_2) state via the 1078- and 1663-keV transitions. Two more levels at even higher excitation energies were detected. An extended model space is necessary to explain them either by lifting of a $1g_{9/2}$ neutron into the $2d_{5/2}$ orbit or by exciting a proton from the $2p_{3/2}$ or $1f_{5/2}$ shells into the $2p_{1/2}$ shell. The first possibility is unlikely as the energy needed amounts to several MeV, as shown by the calculations of Kabadiyski *et al.* in the case of ^{90}Mo [18]. The promotion of a $1f_{5/2}$ proton into the empty $2p_{1/2}$ shell provides a spin gain of $3\hbar$ and is favored by the Nordheim rules and the measured DCO ratios of the 462- and 1442-keV transitions. As the extra $\pi(p_{3/2})^{-1}\pi(p_{1/2})^1$ pair should first couple to $1\hbar$, the 9805-keV level could also have seniority $v = 10$ $[\pi(p_{3/2})^{-1}\pi(p_{1/2})^1]_1\pi(g_{9/2})^5_{25/2}\nu(g_{9/2})^{-3}_{21/2}$ and $[\pi(f_{5/2})^{-1}\pi(p_{1/2})^1]_1\pi(g_{9/2})^5_{25/2}\nu(g_{9/2})^{-3}_{21/2}$ 24^+ partitions.

2. *Negative parity states*

In general, negative parity can be produced by either one proton or one neutron in the $2p_{1/2}$ orbital and the other valence nucleons/holes moving in the $1g_{9/2}$ orbital. Table III lists the predicted main components in the wave functions of negative parity states.

(*i*) v=2. The lowest negative parity states in ^{90}Tc are generated by a proton in the $2p_{1/2}$ orbital. The existence of the 4^- and 5^- states can be explained by coupling a $1g_{9/2}$ neutron hole to that proton. This simple configuration contributes about 50% to the wave function. The 4^- state has a sizable $\pi(g_{9/2})^1\nu(p_{1/2})^{-1}$ component, which is associated with the $1/2^-$ state in ^{89}Mo. We mention here that contributions as $\pi(p_{3/2})^{-1}\nu(g_{9/2})^{-1}$ or $\pi(f_{5/2})^{-1}\nu(g_{9/2})^{-1}$ to the negative parity states are likely but not considered within our very restricted model space.

(*ii*) $v = 4$. The maximum spin value with seniority $v = 4$ is 13^-. The calculations predict the $\pi(p_{1/2})^1\pi(g_{9/2})^2_i\nu(g_{9/2})^{-1}$, $i = 2, 4, 6, 8$ configurations to be yrast; the 7^-, 9^-, 11^-_1, 12^-_1, and 13^-_1 states should contain about 50% of this component. In contrast, the 11^-_2, 12^-_2, and 13^-_3 states are supposed to have main partitions of $\pi(g_{9/2})^1\nu(p_{1/2})^{-1}\nu(g_{9/2})^{-2}_{6,8}$. As an example, the components of the wave functions of the two 12^- states are presented in Table III. The 12^-_1 state in ^{90}Tc, the 5^- state in ^{90}Mo and the $17/2^-_1$ states in ^{89}Mo and ^{91}Tc have a $2p_{1/2}$ proton. The $17/2^-_2$ state in ^{89}Mo has a 61% $\nu(p_{1/2})^{-1}\nu(g_{9/2})^{-2}_8$ component. The coupling of a $1g_{9/2}$ proton to that configuration provides a 12^- and 13^- state in ^{90}Tc and as expected, the 12^-_2 state has a 59% $\pi(g_{9/2})^1\nu(p_{1/2})^{-1}\nu(g_{9/2})^{-2}_8$ partition. It should be noted that the strong 218-keV $13^-_1 \rightarrow 12^-_1$ $M1$ branch of $b = 0.55(3)$ may be associated with a spin recoupling within the $v = 4$ seniority scheme.

(*iii*) $v \geq 6$. On the basis of seniority arguments one may expect the levels up to $19\hbar$ to have $v_\pi = v_\nu = 3$ $\pi(p_{1/2})^1\pi(g_{9/2})^2_8\nu(g_{9/2})^{-3}_i$, i=13/2,17/2,21/2 configurations, but already the 15^- state contains a 36% v_π=5 $\pi(p_{1/2})^1\pi(g_{9/2})^4_{10}\nu(g_{9/2})^{-1}$ partition. Up to spin $I = 21\hbar$ the $\pi(p_{1/2})^1\pi(g_{9/2})^4_{10}\nu(g_{9/2})^{-3}_i$, i=13/2,17/2,21/2 are the most important components. The levels with even and odd spins in that region are predicted to be nearly degenerated and they are not observed in the experiment, either. This is the reason for the strong $21^- \rightarrow 19^- \rightarrow 17^- \rightarrow 15^-$ $E2$ cascade in contrast to the odd-A neighbors. In these nuclei more and different coupling schemes are predicted resulting in a ΔI=1 $M1$ decay pattern as discussed in [17]. Finally, the (23^-) state is explained as a completely aligned seniority $v = 8$ $\pi(p_{1/2})^1\pi(g_{9/2})^4_{12}\nu(g_{9/2})^{-3}_{21/2}$ configuration. The two fast $M1$ transitions with 955 and 446 keV are once more interpreted as a spin recoupling cascade.

TABLE III. Wave functions of negative parity states in ^{89,90}Mo and ^{90,91}Tc.

Isotope	Spin [$\hbar$]	Wave function Ψ		Contribution [%]
^{89}Mo	$1/2^-$		$\nu(p_{1/2})^{-1}$	72.0
^{91}Tc	$1/2^-$	$\pi(p_{1/2})^1$		74.7
^{90}Tc	4^-	$\pi(p_{1/2})^1$	$\nu(g_{9/2})^{-1}$	40.4
		$\pi(g_{9/2})^1$	$\nu(p_{1/2})^{-1}$	11.0
	5^-	$\pi(p_{1/2})^1$	$\nu(g_{9/2})^{-1}$	51.7
		$\pi(g_{9/2})^1$	$\nu(p_{1/2})^{-1}$	1.7
^{90}Mo	5^-	$[\pi(p_{1/2})^1\pi(g_{9/2})^1]_5$		75.8
			$[\nu(p_{1/2})^{-1}\nu(g_{9/2})^{-1}]_5$	2.2
^{89}Mo	$17/2^-$	$[\pi(p_{1/2})^1\pi(g_{9/2})^1]_{4,5}$	$\nu(g_{9/2})^{-1}$	62.4
			$[\nu(p_{1/2})^{-1}\nu(g_{9/2})^{-2}_8]_{17/2}$	2.7
	$17/2^-_2$	$[\pi(p_{1/2})^1\pi(g_{9/2})^1]_{4,5}$	$\nu(g_{9/2})^{-1}$	1.9
			$[\nu(p_{1/2})^{-1}\nu(g_{9/2})^{-2}_8]_{17/2}$	61.0
^{91}Tc	$17/2^-$	$[\pi(p_{1/2})^1\pi(g_{9/2})^2_8]_{17/2}$		62.6
		$\pi(g_{9/2})^1$	$[\nu(p_{1/2})^{-1}\nu(g_{9/2})^{-1}]_{4,5}$	3.4
^{90}Tc	12^-	$[\pi(p_{1/2})^1\pi(g_{9/2})^2_8]_{17/2}$	$\nu(g_{9/2})^{-1}$	51.1
		$\pi(g_{9/2})^1$	$[\nu(p_{1/2})^{-1}\nu(g_{9/2})^{-2}_8]_{17/2}$	2.1
	12^-_2	$[\pi(p_{1/2})^1\pi(g_{9/2})^2_8]_{17/2}$	$\nu(g_{9/2})^{-1}$	0.7
		$\pi(g_{9/2})^1$	$[\nu(p_{1/2})^{-1}\nu(g_{9/2})^{-2}_8]_{17/2}$	58.8
^{90}Mo	17^-	$[\pi(p_{1/2})^1\pi(g_{9/2})^3_{17/2}]_9$	$\nu(g_{9/2})^{-2}_8$	44.1
^{89}Mo	$39/2^-$	$[\pi(p_{1/2})^1\pi(g_{9/2})^3_{17/2}]_9$	$\nu(g_{9/2})^{-3}_{21/2}$	43.2
^{91}Tc	$37/2^-$	$[\pi(p_{1/2})^1\pi(g_{9/2})^4_{10}]_{21/2}$	$\nu(g_{9/2})^{-2}_8$	80.1
^{90}Tc	21^-	$[\pi(p_{1/2})^1\pi(g_{9/2})^4_{10}]_{21/2}$	$\nu(g_{9/2})^{-3}_{21/2}$	65.9

V. CONCLUSIONS

To summarize we have identified excited states in ^{90}Tc via particle-$\gamma\gamma$ coincidences. We deduced a comprehensive and complex level scheme by $n\gamma\gamma$ coincidences, intensity and summed energy relations. The level scheme is built upon an 8^+ state, which most probably is the ground state. For approximately half of the 45 levels identified, definite spin and parity assignments were made. Some features of the level scheme can be understood in terms of energy level systematics with neighboring nuclei. RITSSCHIL shell model calculations in a limited model space reveal detailed insight into the origin of the individual states. The shell model with the eight valence particles/holes moving in the $2p_{1/2}$ and $1g_{9/2}$ orbitals provides a good description of the energies of states below 9 MeV excitation energy. Many states are proposed to have pure aligned seniority configurations and are expected to decay via strong and fast $M1$ transitions. Other states should have weak decay branches due to different proton and neutron seniorities. In the high spin region of the positive parity band our very restricted configuration space is exceeded. The 462–1442-keV sequence upon the 9342-keV level may be explained by promoting a proton from the $1f_{5/2}$ into the $2p_{1/2}$ orbital. In the low spin regime also some vibrational excitations may take place. Lifetime and magnetic moment measurements are in progress to test the proposed wave functions.

ACKNOWLEDGMENTS

This research was supported by Deutsches BMFT under contract 06GÖ451 and 06OK143. The help of F. Cristancho, A. Jungclaus, T. Mylaeus, and S. Skoda during the experiments is gratefully acknowledged. The authors would also like to thank the crew and staff of the accelerators at Berlin and Köln for their support.

[1] C.J. Lister, P.J. Ennis, A.A. Chishti, B.J. Varley, W. Gelletly, H.G. Price, and A.N. James, Phys. Rev. C **42**, R1191 (1990).

[2] W. Fieber, K. Bharuth-Ram, J. Heese, F. Cristancho, C.J. Gross, K.P. Lieb, S. Skoda, and J. Eberth, Z. Phys. A **332**, 363 (1989).

[3] L. Lühmann, K.P. Lieb, C.J. Lister, B.J. Varley, J.W. Olness, and H.G. Price, Europhys. Lett. **1**, 623 (1986).

[4] C.J. Gross, J. Heese, K.P. Lieb, L. Lühmann, B. Wörmann, A.A. Chishti, W. Gelletly, C.J. Lister, J.H. McNeill, and B.J. Varley, Z. Phys. A **331**, 361 (1988).

[5] F. Cristancho, C.J. Gross, K.P. Lieb, D. Rudolph, Ö.

Skeppstedt, M.A. Bentley, W. Gelletly, H.G. Price, J. Simpson, J.L. Durell, B.J. Varley, and S. Rastikerdar, Nucl. Phys. **A540**, 307 (1992).
[6] B. Wörmann, K.P. Lieb, R. Diller, L. Lühmann, J. Keinonen, L. Cleemann, and J. Eberth, Nucl. Phys. **A431**, 170 (1984).
[7] A. Dewald, U. Kaup, W. Gast, A. Gelberg, H.-W. Schuh, K.O. Zell, and P. von Brentano, Phys. Rev. C **25**, 226 (1982).
[8] R. Diller, K.P. Lieb, L. Lühmann, T. Osipowicz, P. Sona, B. Wörmann, L. Cleemann, and J. Eberth, Z. Phys. A **321**, 659 (1985).
[9] E.K. Warburton, C.J. Lister, J.W. Olness, P.E. Hausstein, S.K. Sara, D.E. Alburger, J.A. Becker, R.A. Dewburry, and R.A. Naumann, Phys. Rev. C **31**, 1184 (1985).
[10] K. Oxorn, S.K. Mark, J.E. Kitching, and S.S.M. Wong, Z. Phys. A **321**, 485 (1985).
[11] C.J. Gross, D. Rudolph, K.P. Lieb, W. Gelletly, M.A. Bentley, H.G. Price, J. Simpson, D.J. Blumenthal, P.J. Ennis, C.J. Lister, Ch. Winter, J.L. Durell, B.J. Varley, S. Rastikerdar, and Ö. Skeppstedt, Nucl. Phys. **A535**, 203 (1991).
[12] A. Jungclaus, K.P. Lieb, C.J. Gross, J. Heese, D. Rudolph, D.J. Blumenthal, P. Chowdhury, P.J. Ennis, C.J. Lister, Ch. Winter, J. Eberth, S. Skoda, M.A. Bentley, W. Gelletly, and B.J. Varley, Z. Phys. A **340**, 125 (1991).
[13] W. Gelletly, M.A. Bentley, H.G. Price, J. Simpson, C.J. Gross, J.L. Durell, B.J. Varley, Ö. Skeppstedt, and S. Rastikerdar, Phys. Lett. B **253**, 287 (1991).
[14] C.J. Gross, W. Gelletly, M.A. Bentley, H.G. Price, J. Simpson, K.P. Lieb, D. Rudolph, J.L. Durell, and S. Rastikerdar, Phys. Rev C **44**, R2253 (1991).
[15] Ch. Winter, D.J. Blumenthal, P. Chowdhury, B. Crowell, P.J. Ennis, S.J. Freeman, C.J. Lister, C.J. Gross, J. Heese, A. Jungclaus, K.P. Lieb, D. Rudolph, M.A. Bentley, W. Gelletly, J.L. Durell, and B.J. Varley, Nucl. Phys. **A535**, 137 (1991).
[16] M. Weiszflog, K.P. Lieb, F. Cristancho, C.J. Gross, A. Jungclaus, D. Rudolph, H. Grawe, J. Heese, K.H. Maier, R. Schubart, J. Eberth, and S. Skoda, Z. Phys. A **342**, 257 (1992).
[17] M. Weiszflog, D. Rudolph, C.J. Gross, M.K. Kabadiyski, K.P. Lieb, H. Grawe, J. Heese, K.H. Maier, and J. Eberth, Z. Phys. A **344**, 395 (1993).
[18] M.K. Kabadiyski, F. Cristancho, C.J. Gross, A. Jungclaus, K.P. Lieb, D. Rudolph, H. Grawe, J. Heese, K.H. Maier, J. Eberth, S. Skoda, W.-T. Chou, and E.K. Warburton, Z. Phys. A **343**, 165 (1992).
[19] D. Rudolph, F. Cristancho, C.J. Gross, A. Jungclaus, K.P. Lieb, M.A. Bentley, W. Gelletly, J. Simpson, H. Grawe, J. Heese, K.H. Maier, J. Eberth, S. Skoda, J.L. Durell, B.J. Varley, D.J. Blumenthal, C.J. Lister, and S. Rastikerdar, J. Phys. G **17**, L113 (1991).
[20] D. Rudolph, F. Cristancho, C.J. Gross, A. Jungclaus, K.P. Lieb, H. Grawe, J. Heese, K.H. Maier, J. Eberth, and S. Skoda, Z. Phys. A **342**, 121 (1992).
[21] S.E. Arnell, S. Sjöberg, E. Wallander, A. Nilsson, Z.P. Sawa, and G. Finnes, Z. Phys. A **289**, 89 (1978).
[22] D. Bucurescu, G. Constantinescu, D. Cutoiu, M. Ivaşcu, N.V. Zamfir, and A. Abdel Haliem, J. Phys. G **10**, 1189 (1984).
[23] R. Gross and A. Frenkel, Nucl. Phys. **A267**, 85 (1976).
[24] A. Amusa and R.D. Lawson, Z. Phys. A **314**, 205 (1983).
[25] K. Oxorn and S.K. Mark, Z. Phys. A **303**, 63 (1981).
[26] S. Wen, H. Zheng, G.S. Li, S.G. Li, P.K. Weng, P.F. Hua, L.K. Zhang, P.S. Yu, G.J. Yuan, and C.X. Yang, in International Nuclear Physics Conference, Wiesbaden, 1992, edited by U. Grundinger (to be published).
[27] R.M. Lieder, H. Jaeger, A. Neskakis, and T. Venkova, Nucl. Instrum. Methods **220**, 363 (1984).
[28] D. Alber, H. Grawe, H. Haas, and B. Spellmeyer, Nucl. Instrum. Methods **263**, 401 (1988).
[29] A. Gavron, Phys. Rev. C **21**, 230 (1980).
[30] K. Schreckenbach, computer program LEFIT, Institut Laue Langevin (unpublished).
[31] T. Yamazaki, At. Data Nucl. Data Tables **3**, 1 (1967).
[32] E.F. Moore, Computer Program AD, Florida State University (unpublished).
[33] D. Weil, Computer Program CHIPLO, University of Cologne (unpublished).
[34] D.C. Camp and A.L. van Lehn, Nucl. Instrum. Methods **76**, 192 (1969).
[35] H.J. Rose and D.M. Brink, Rev. Mod. Phys. **39**, 306 (1967).
[36] A.R. Poletti and E.K. Warburton, Phys. Rev. **137**, B595 (1965).
[37] M.K. Kabadiyski, K.P. Lieb, and D. Rudolph (unpublished).
[38] R. Iafigliola, R. Turcotte, R.B. Moore, and J.K.P. Lee, Nucl. Phys. **A182**, 400 (1972).
[39] E.K. Warburton and D.E. Alburger, Phys. Rev. C **26**, 2595 (1982).
[40] S.I. Hayakawa, S.K. Mark, J.K. Lee, J.E. Kitching, G.C. Ball, and W.G. Davies, Nucl. Phys. **A199**, 560 (1973).
[41] S. Chattopadhyay, H.C. Jain, J.A. Sheikh, Y.K. Agarwal, and M.L. Jhingan, Phys. Rev. C **47**, R1 (1993).
[42] C.A. Fields, F.W.N. de Boer, J.J. Kraushaar, R.A. Ristinen, L.E. Samuelson, and E. Sugarbaker, Nucl. Phys. **A363**, 311 (1981).
[43] C.A. Fields, F.W.N. de Boer, and B.J. Diana, Nucl. Phys. **A401**, 117 (1983).
[44] P. Komninos, E. Nolte, and P. Blasi, Z. Phys. A **314**, 135 (1983).
[45] I. Talmi and I. Unna, Nucl. Phys. **19**, 225 (1960).
[46] D.H. Gloeckner and F.J.D. Serduke, Nucl. Phys. **A220**, 477 (1974).
[47] D. Zwarts, Comput. Phys. Commun. **38**, 365 (1985).
[48] A.I. Kucharska, J. Billowes, and C.J. Lister, J. Phys. G **15**, 1039 (1989).
[49] J. Billowes, private communication.
[50] D. Häusser, T. Faestermann, I.S. Towner, T.K. Alexander, H.R. Andrews, J.R. Beene, D. Horn, and D. Ward, Hyperfine Interact. **4**, 196 (1978).